INTERNATIONAL JOURNAL OF HYDROGEN ENERGY 42 (2017) 5306–5314

Available online at www.sciencedirect.com

ScienceDirect

journal homepage: www.elsevier.com/locate/he

Interactions near the triple-phase boundaries metal/glass/air in planar solid oxide fuel cells

M. Fakouri Hasanabadi, A.H. Kokabi*, A. Nemati, S. Zinatlou Ajabshir

Department of Materials Science and Engineering, Sharif University of Technology, Azadi Avenue, P. O. Box 11155-9466, Tehran, Iran

ARTICLE INFO

Article history:
Received 5 September 2016
Received in revised form
3 December 2016
Accepted 10 January 2017
Available online 1 February 2017

Keywords:
Solid oxide fuel cells
Triple-phase boundaries
Ferritic stainless steel
Glass
Air side

ABSTRACT

The possible interactions near the triple-phase boundaries (TPB) metal/glass/air, and their effects on joint strength are investigated. Two types of samples (joined couples and glass coated coupons) are prepared with the coupon of AISI 430 (nickel plated and uncoated) and a slurry of compliant silicate sealing glass (SCN-1). The joined and coated samples are heated at 850 °C for 1000 h in air. The joined couples are cooled using two different schedules and then tested in uniaxial tension. For investigating the metal-oxides precipitation procedure in glass near the TPB, glass coated coupons are either cooled at the rate of 5 °C min^{-1} or water-quenched from aging temperature. The mechanical test results and microstructural observations show that the spread and accelerated breakaway oxidation near TPB, which is due to continuous oxidation and dissolution of ferritic stainless steel (FSS) into the glass, leads to decreased and scattered low temperature joint strengths.
© 2017 Hydrogen Energy Publications LLC. Published by Elsevier Ltd. All rights reserved.

Introduction

Solid oxide fuel cell (SOFC) is a device that generates electricity directly from chemical reactions between fuel and oxidant. The planar SOFCs (pSOFCs) with metallic interconnects can be categorized as the second generation SOFCs after the sealless tubular cells and the planar cells with ceramic interconnects. Metallic interconnects have low fabrication costs, better thermal and electrical conductivity, and higher toughness. One of the major challenges for commercializing pSOFCs concerns sealant materials. These sealants must prevent fuel–oxidant mixing, provide electrical insulation of the stack layers and also have limited interaction with other components for long times (5000–40,000 h) at high temperatures (between 600 °C and 1000 °C) [1].

In the last two decades, extensive research has been carried out on interactions between glasses (or glass-ceramics) and ferritic stainless steels (FSSs) as sealant and interconnect, respectively. It has been shown that the extent and nature of the metal/glass interactions in the interior region of the joints are not the same as the edge region. Yang et al. [2,3] studied the interaction between barium-containing glass and FSS. They found that the detrimental barium chromate ($BaCrO_4$) phase is formed near the triple-phase boundaries (TPB) metal/glass/air and not at the interior metal/glass interfaces. Haanappel and Menzler et al. [4–9] investigated the interactions between different glass sealant–alloy combinations under different atmospheric conditions (air, humidified hydrogen and humidified hydrogen/air dual atmosphere). They reported that during exposing at least one side of glass–ceramics containing minor amounts of PbO to

* *Corresponding author*. Fax: +98 21 6600 5717.
E-mail addresses: fakouri@mehr.sharif.ir (M. Fakouri Hasanabadi), kokabi@sharif.edu (A.H. Kokabi), nemati@sharif.edu (A. Nemati), zinatlou_sina@mehr.sharif.edu (S. Zinatlou Ajabshir).
http://dx.doi.org/10.1016/j.ijhydene.2017.01.065
0360-3199/© 2017 Hydrogen Energy Publications LLC. Published by Elsevier Ltd. All rights reserved.

humidified hydrogen, excessive corrosion of the FSS may occur, which eventually results in a short-circuiting between adjacent interconnector plates. It appeared that excessive internal Cr oxidation of FSS often occurred near the hydrogen side and sometimes was accompanied by external Fe-oxide formation (a so-called breakaway oxidation) near the air side. Similar observations of Ba or Sr chromates formation [10–12] and breakaway oxidation [13–17] at the sealing edges exposed to air and also internal Cr oxidation near the hydrogen side [11,18–20] have also been reported in several other studies.

In addition to modification of glass and FSS compositions [21–23], many other efforts have been made on the modification of FSS surface to reduce the detrimental interactions, including pre-oxidation [16,24], aluminizing [25] and applying protective coating [26,27]. Recently, the behavior of nickel layer on the FSS surface has also been investigated under SOFC conditions [28–35].

Our recent work [36] revealed some severe corrosion of FSS near TPB of AISI 430/SCN-1 glass/air during a short heat-treatment (850 °C/100 h) which could be lessened by an intermediate nickel layer. However, inward diffusion of a portion of Ni through FSS led to rapid loss of adhesion strength all over the joined area. Although non-uniform diffusion of Ni into FSS (and thus non-uniform thermal stress generation) was scrutinized, a more comprehensive experimental study of interaction near TPB is still needed.

In this paper, attention has been focused on the TPB of AISI 430/SCN-1 glass/air to evaluate chemical and mechanical aspects of interactions at 850 °C for longer duration of heat treatment (1000 h).

Experimental

Materials and sample preparation

Commercial alkali silicate glass (SCN-1, Par-e-tavous, Khorasan-e-razavi, Iran) was used. This glass contains alkaline earth elements, mainly in the form of BaO (8.23 mol%) and CaO (3.34 mol%), alkalis of K_2O (10.0 mol%) and Na_2O (7.3 mol %), Al_2O_3 (2.8 mol%), and some impurities (less than 1%) of Fe, Mg and Ti with the balance of SiO_2. The glass transition temperature (T_g), softening point (T_d), and coefficient of thermal expansion (CTE) were about 470 °C, 550 °C and $11 \times 10^{-6}\,°C^{-1}$, respectively. The details of SCN-1 behavior as a compliant sealing glass for solid oxide fuel cell applications has been reported earlier [37–40]. SCN-1 as a non-crystallizing compliant sealing glass allows us to focus on interfacial interactions for seal strength investigation.

AISI 430 is a commercial FSS (Hardox, Oxelösund, Sweden) containing Cr (17.5 wt%), Ni (0.13 wt%), C (0.05 wt%), Mn (0.25 wt%), Cu (0.13 wt%) and Si (0.15 wt%) with the balance of Fe. In this study, FSS sheets with a thickness of 0.5 mm were used in two states of 10 μm thick Ni-plated and uncoated. The coating with thickness of 10 μm is chosen because it has been reported that FSS with 8–10 μm thick nickel coating performs better under SOFC atmospheres [32,34]. Detailed information about the electroplating procedure is described in Ref. [36].

For tensile tests, FSS/glass/FSS sandwiches (joined couples) were prepared. The thickness of glass after joining was 0.5 ± 0.05 mm. To prepare samples, a given volume of glass slurry was applied onto the FSS coupons surface with dimensions of 1×1 cm^2. The slurry was a mixture of glass powder and additives (0.2 wt.% borax, 0.2 wt.% sodium nitrate, 1 wt.% kaolin, and 0.5 wt.% silica) dispersed in deionized water by ball-mill treatment. After applying the slurry, the samples were dried at 70 °C for 15 min. The dried samples were then thermally aged at 850 °C for 1000 h in air. The heating and cooling rates were about 5 °C min^{-1}. Significant thermal stress reduction at the glass/metal interface can be achieved by reducing the cooling rate through the annealing range of glass [41]. Regarding to approximate annealing temperature for SCN-1 (447 °C) [42], some samples were cooled from 450 °C to room temperature at a rate of 1 °C min^{-1}.

In addition to the joined couples, some samples were prepared in the form of glass coated FSS coupons. These samples were either cooled at the rate of 5 °C min^{-1} or water-quenched from aging temperature for investigating the metal-oxides precipitation process in glass near the TPB. The thickness of glass coating was 0.3 ± 0.5 mm.

Mechanical testing and microstructural characterization

For joint strength tests, the joined couples were glued to a self-alignment fixture. The assembly was then tested in uniaxial tension with a cross-head speed of 0.5 mm min^{-1} in ambient conditions. Tensile tests were carried out using a Hounsfield H10KS with a 1000 N load cell. Detailed information about test principles and equipment is given in Ref. [36]. For each condition, 20 samples were tested, and results were analyzed using two-parameter Weibull probabilistic equation which is shown below

$$P_f = 1 - \exp\left[-\left(\frac{\sigma}{\sigma_\theta}\right)^m\right]$$

where P_f is the failure probability for an applied stress σ, σ_θ is the Weibull characteristic strength (which corresponds to $P_f = 63.2\%$) and m is the Weibull modulus. Here, the Weibull modulus m is a measure of the degree of strength data scatter. The Weibull parameters (σ_θ and m) were calculated according to ASTM C1239-13.

Some of the samples were also mounted in epoxy and then sectioned and polished for interfacial characterization using optical (Olympus BX51M) and scanning electron microscopes (SEM VEGA∖∖TESCAN-XMU).

Results and discussion

Joint strength

Fracture surface analysis revealed that crack propagation mainly occurs along the glass/metal interface. It means that the joint strength is controlled by glass/metal adhesion. The two-parameter Weibull distribution of fracture strength for the joined couples is shown in Fig. 1. The joint couples with Ni-plated and uncoated coupons are denoted as N and S,

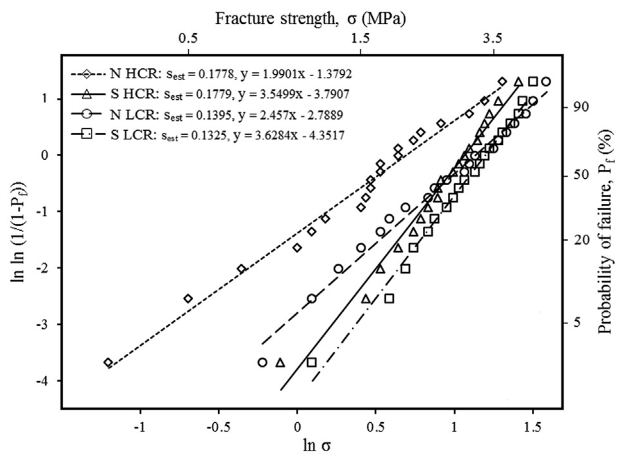

Fig. 1 – Weibull distribution of fracture strengths for N (Ni-plated) and S (uncoated) joined couples prepared at cooling rates of 5 °C min^{-1} (HCR) and 1 °C min^{-1} (LCR). Here, s_{est} denotes the standard deviation of the estimate for linear regression.

respectively. As it is seen, S joint couples exhibited a greater strength than N ones. Also it can be seen in Fig. 1 that the reduction in cooling rate in order to increase the strength of N joint couples was more effective than for S ones. These observations confirm the presence of significant thermal stresses at the Ni-plated FSS/glass interface. Indeed, diffusion of a portion of the Ni coating into FSS during aging leads to extension of unstable austenite zones near the interface. During cooling, the austenite to ferrite transformation is followed by a significant volume expansion in a short temperature range which leads to increased residual stress or crack formation at the interface.

It can be seen in Table 1 that all m values, especially for more rapidly cooled N joint couples, are low. Whilst we observed lower scatter as well as higher value for fracture strength of joint couples which heat treated for shorter durations [36]. Weibull modulus m is related to uniformity of the microstructure, including flaws, grain size, and inclusions [43]. Here, the wide distributions of strength and hence low m value can be related to the flaws and inclusions caused by detrimental interactions near TPB, and could also be intensified by non-uniform residual stresses at the Ni-plated FSS/glass interfaces.

Chemical interactions

Fig. 2 shows the metal/glass interfaces away from TPB. It is clearly evident that Cr diffused to surfaces of both uncoated and Ni-plated FSS and caused formation of a Cr-rich oxide at the interfaces. Although a slight diffusion of Cr into glass (2.4 μm and 1.2 μm for uncoated and Ni-plated samples respectively) can be observed, there is no evidence of Fe and Ni presence in glass. Also, the visible mild corrosion of either uncoated or Ni-plated FSS (with about 5- and 10-μm-thick oxide layers respectively) demonstrates the limited metal/glass interactions along the interior interfaces.

The limitation in interactions is due to lack of access to oxygen from air. In the absence of oxygen, Cr and Mn continuously diffuse into the interface and form an insoluble (Cr, Mn) oxide by reduction of thermodynamically less stable oxides. In addition to surface oxides, the dissolved metal oxides and some of modifier oxides of glass can also be reduced and precipitate from glass. Therefore such redox reactions can gradually deplete the glass of dissolved Fe and Ni oxides [36].

Fig. 3a and b shows the cross-sectional micrographs of uncoated FSS/glass interface near TPB. It is seen that FSS was severely corroded (to a depth of 66 μm relative to interior metal/glass interface) in the vicinity of SCN-1 glass and also a large amount of Fe-rich nodules grew outwardly and were distributed in the glass. Fig. 3c reveals a low Cr concentration gradient in FSS near the corroded region.

The observations demonstrate the occurrence of breakaway oxidation underneath the glass near TPB. The breakaway oxidation tends to take place when Cr consumption at the alloy surface is faster than Cr diffusion from the bulk. Under these conditions, Cr is depleted down to the critical concentration (16 wt.%) in the underlying alloy. Thus protective chromia layer can no longer be retained and consequently external Fe-rich oxide starts to form [16,17,45].

Fig. 4a and b shows uncoated FSS/glass interfaces near TPB for glass coated coupons cooled at a rate of 5 °C min^{-1} and water-quenched, respectively. The flake-like particles of Fe-oxides are seen near the outer surface of glass in both coupons. The higher magnification images (Fig. 4c and d) reveal that, unlike the slow cooled coupon, there are some finer flakes amidst the coarse ones in the quenched coupon. Also, no Cr-diffusion into this region of glass can be detected by EDS analysis of both coupons (Fig. 4e and f).

The evidences indicate that a significant amount of Fe-oxide can be dissolved in glass near TPB during aging and then precipitate during cooling. The dissolved metal-oxides in glass normally tend to crystalize during cooling through

Table 1 – Weibull parameters (σ_0 and m), average strength (σ_{ave}), standard deviation (s), and uncertainty (u) of measurement with a confidence interval of 95%.

Joined couple	σ_0 (MPa)	s (σ_0)[a] (MPa)	u (σ_0) (MPa)	m	s (m)[a]	σ_{ave} (MPa)	s (σ_{ave}) (MPa)	u (σ_{ave}) (MPa)
N HCR	2.0	±0.2	±0.1	2.0	±0.4	1.8	±0.9	±0.4
S HCR	2.9	±0.2	±0.1	3.5	±0.8	2.6	±0.8	±0.4
N LCR	3.1	±0.3	±0.1	2.5	±0.5	2.8	±1.2	±0.5
S LCR	3.3	±0.2	±0.1	3.6	±0.8	3.0	±0.9	±0.4

[a] Details on the calculation are given in Ref. [44].

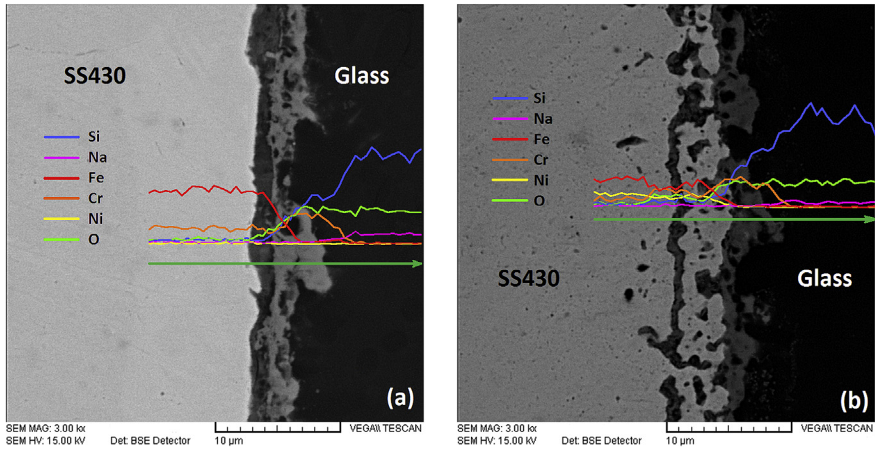

Fig. 2 – EDS line scans across the interior SCN-1 glass interface with uncoated (a) and Ni-plated (b) AISI 430 for joint couples aged at 850 °C for 1000 h in air followed by cooling at a rate of 5 °C min^{-1}.

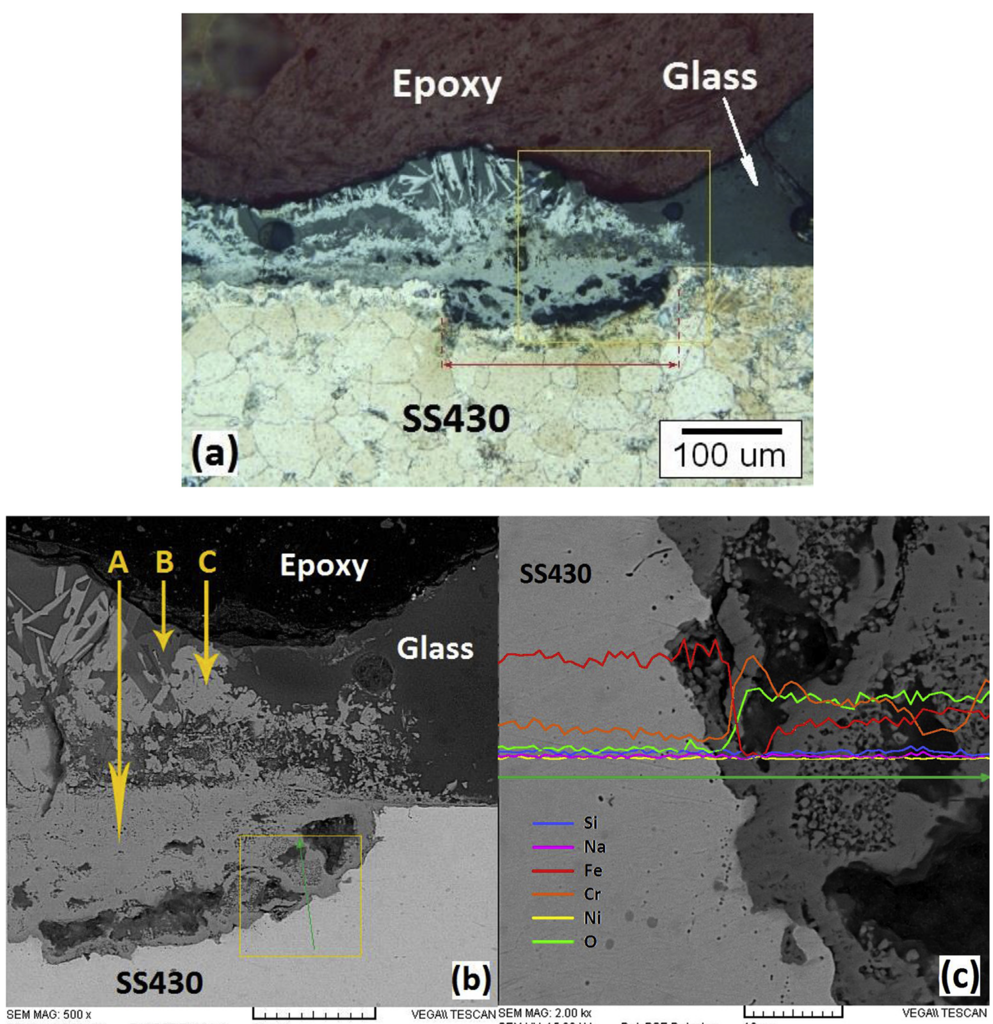

Fig. 3 – Optical (a) and Backscattered electron SEM micrograph of uncoated AISI 430/SCN-1 glass interface near TPB after heat treating at 850 °C for 1000 h in air (b), EDS line scan across the uncorroded/corroded boundary in the area indicated in Fig. 3a with a 90° clockwise rotation (c). A: (Fe, Cr) oxide, B: Fe-oxide underneath the glass, C: Fe-oxide.

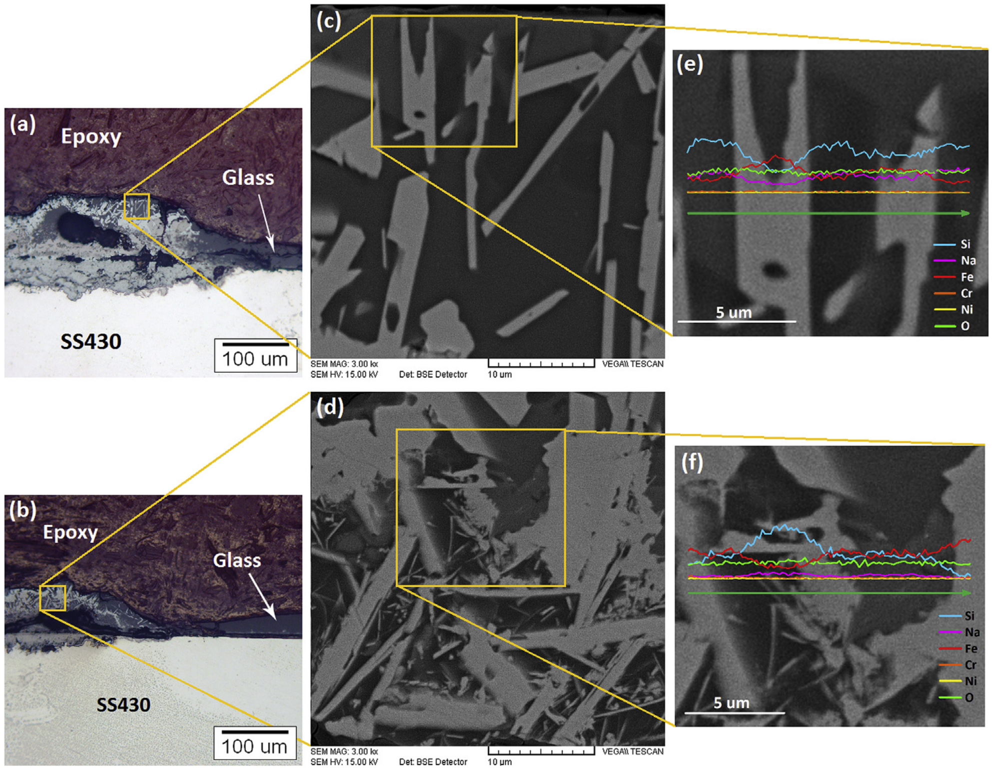

Fig. 4 – Cross-sectional optical micrographs of uncoated AISI 430/SCN-1 glass interface near TPB after heat treating at 850 °C for 1000 h in air followed by cooling at a rate of 5 °C min^{-1} (a) and water-quenching (b) to ambient temperature. Magnified views of area indicated in a (c) and b (d). EDS line scans in the area indicated in c (e) and d (f).

nucleation and growth procedure. According to thermodynamic principle, nucleation process tends to be heterogeneous and the nuclei usually form on the interface which is the reason why the flakes exist as parts of metal substrate [46,47]. The increased cooling rate leads to formation of a large number of homogeneous nuclei and consequently decreases the size of final flakes.

At TPBs, the activity of oxygen is high due to more access to air, thus the competition for oxygen is diminished [48,49]. Therefore, a high amount of (Fe, Cr) oxide can be continuously produced at the FSS surfaces [50]. Compared to Cr_2O_3, the Fe-oxide has a higher tendency to be dissolved in the glass [51]; hence, it leads to continuous breakdown of surface oxide layer. This phenomenon increases the Cr consumption at the FSS surface and results in breakaway oxidation. The resulting voluminous products lead to local bulging of the FSS and push away the glass from the surface. Therefore, oxygen penetrates more readily into metal/glass interface from air, and in this way the breakaway oxidation spreads to interior interfaces [5–7]. As it is seen in Fig. 3a, the intensified corrosion has reached its maximum (66 μm depth) at the zone indicated by red (in the web version) line, where there is enough access to oxygen as well as plenty of glass for, respectively, oxidation and dissolution of FSS.

As discussed by other authors [13,15] the enrichment of Na in the oxide scale would suggest the formation of Na_2CrO_4. The high vapor pressure of this alkali chromate can result in its vaporization which can increase the Cr consumption at the FSS surface. However, the results of the present study showed that there was no trace of Na in oxidation products. Bram et al. [16] reported that pre-oxidation leads to the homogeneous formation of a protective chromia-based oxide scale on the FSS surface, which reliably avoids breakaway oxidation. The pre-oxidation in a reducing atmosphere with low oxygen activity in order to form of a Fe-free chromia layer on the FSS surface can be the subject of further research.

Fig. 5a shows the cross-sectional optical micrograph of Ni-plated FSS/glass interface near TPB after etching with marble reagent. The diffusion of Ni through the ferritic structure (mustard grains) leads to an increase in the thickness of austenite phase (bright white layer) to about 85 μm. The depth of corrosion underneath the glass has reached up to 23 μm relative to interior metal/glass interface, and corrosion products are gradually decreased from metal/air to interior metal/glass interfaces. Therefore, it can be said that there is no intensified corrosion of FSS near TPB. The chemical composition of flake-like particles (spot#1 in Fig. 5b) which have grown towards the glass is given in Table 2. The EDS analysis across the corrosion products near TPB (Fig. 5c) confirms that the Ni-coating was completely oxidized and some Cr-rich oxide (indicated by green (in the web version) arrows) formed underneath and inside it. Also it can be seen that some dendrites of (Fe, Ni) oxide (indicated by red arrow) formed in glass, next to the coating.

The Ni-rich dendrites and flakes and also Ni-free glass show that Ni-oxide can be dissolved in glass and precipitates

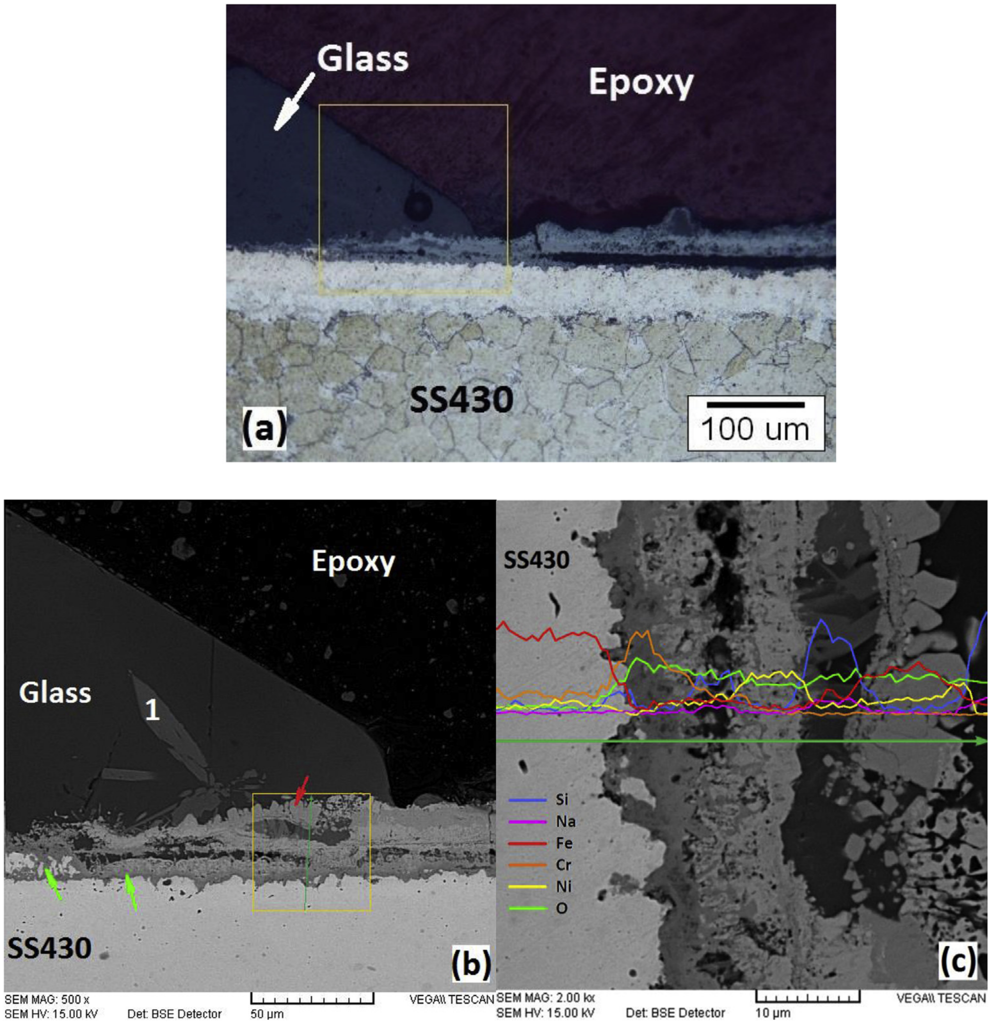

Fig. 5 – Optical (a) and Backscattered electron SEM micrograph of Ni-plated AISI 430/SCN-1 glass interface near TPB after heat treating at 850 °C for 1000 h in air (b), EDS line scan across the interfaces in the area indicated in Fig. 4a with a 90° clockwise rotation (c). EDS of spot#1 is given in Table 2.

with other elements through a nucleation and growth procedure. However, the Ni-oxide has a low tendency to be dissolved in glass [51] therefore the oxidation of Ni-coating leads to formation of a semi-stable layer of Ni-oxide on the FSS surface. This oxide layer decelerates Cr-diffusion into metal/glass interface and thus prevents the rapid extension of Cr-depleted region. As a result, Ni-coating inhibits the accelerated breakaway oxidation underneath the glass.

Mismatches in CTE can result in generation of undesirable residual stresses upon cooling. As it seen in Table 3, Ni-oxide has a relatively high CTE mismatch with SCN-1 glass and FFS as well as other oxides. Higher CTE of Ni-oxide results in tensile residual stress during cooling and consequently can lead to crack formation at the interfaces. Therefore, in addition to reduction of effective interface for load bearing, corrosion products increase the CTE mismatches along the interface and lead to decreased and scattered joint strengths. Shaigan et al. [30,31] reported that addition of $LaCrO_3$ particles to Ni-coating may improve the oxidation resistance and reduce the corrosion products.

The acid–base reactions are the main cause of interaction between glass and metal in the presence of oxygen [59]. The metal oxides can be dissolved in oxide glasses by this type of reactions. In general, the intensity and rate of the acid–base reactions is highest when the glass is more acidic [60].

Table 2 – Chemical composition (at.%) of spot#1 in Fig. 4a.

O	Na	Si	Ca	Fe	Ni
68.91	2.74	14.89	5.68	3.52	4.26

Table 3 – Coefficients of thermal expansion (CTE).

Material	CTE ($\times 10^{-6}$ °C^{-1})	Ref.
SCN-1	11	[37]
Fe_2O_3	14.9	[52]
Fe_3O_4	>9.2	[53,54]
FeO	12.1	[52]
NiO	13.9–17.1	[52,55,56]
Cr_2O_3	5.7–9.6	[57]
AISI 430	12.5	[58]

Therefore, compared to Cr_2O_3 as a neutral oxide, FeO and NiO as two basic oxides are more readily dissolved in silicate glass. Accordingly, the less acidic glasses are better choices for reducing the metal/glass interaction near TPB.

Conclusions

1. The spread and accelerated breakaway oxidation near the triple-phase boundaries (TPB) AISI 430/SCN-1 glass/air reduces the effective interface for load bearing and also causes increased stress concentration during loading. This leads to decreased and scattered low temperature joint strengths.
2. The intensified breakaway oxidation underneath the glass near TPB is due to more access to oxygen which leads to continuous oxidation and dissolution of ferritic stainless steel (FSS) into the glass. In this condition, Cr consumption at the FSS surface becomes faster than Cr diffusion from the bulk and Cr is depleted in the underlying alloy. Thus protective chromia layer can no longer be retained and consequently external Fe-rich oxide starts to form.
3. The Ni-coating forms a semi-stable Ni-oxide layer at the metal/glass interface near TPB which can decelerate the outward Cr-diffusion and thus prevents the extension of Cr-depleted region.
4. In Ni-plated samples, inward diffusion of Ni as an austenite stabilizer element leads to extension of unstable austenite zones near the FSS surfaces. Therefore, in addition to high thermal contraction of Ni-oxide near TPB, the austenite to ferrite transformation increases the residual stress at the interface and leads to decreased adhesion strength and scatter in joint strengths. Accordingly, the pure nickel cannot be suitable candidate for protective coating on FSS against the sealing glass for long-term operation of SOFC because its detrimental effects are more significant than positive effect on corroded region extension near the TPB.

Acknowledgements

The authors wish to thank the research board of Sharif University of Technology for financial support and provision of the research facilities used in this work. We also express our gratitude to Iran Board Electronic Company for providing the electroplating requirements.

REFERENCES

[1] Kaur G, Pandey OP, Singh K. Chemical interaction study between lanthanum based different alkaline earth glass sealants with Crofer 22 APU for solid oxide fuel cell applications. Int J Hydrogen Energy 2012;37:3883–9. http://dx.doi.org/10.1016/j.ijhydene.2011.04.104.

[2] Yang Z, Meinhardt KD, Stevenson JW. Chemical compatibility of barium-calcium-aluminosilicate-based sealing glasses with the ferritic stainless steel interconnect in SOFCs. J Electrochem Soc 2003;150:A1095. http://dx.doi.org/10.1149/1.1590325.

[3] Yang Z, Xia G, Meinhardt KD, Weil SK, Stevenson JW. Chemical stability of glass seal interfaces in intermediate temperature solid oxide fuel cells. J Mater Eng Perform 2004;13:327–34. http://dx.doi.org/10.1361/10599490419298.

[4] Haanappel VAC, Shemet V, Vinke IC, Quadakkers WJ. A novel method to evaluate the suitability of glass sealant?alloy combinations under SOFC stack conditions. J Power Sources 2005;141:102–7. http://dx.doi.org/10.1016/j.jpowsour.2004.08.053.

[5] Haanappel VAC, Shemet V, Vinke IC, Gross SM, Koppitz T, Menzler NH, et al. Evaluation of the suitability of various glass sealant – alloy combinations under SOFC stack conditions. J Mater Sci 2005;40:1583–92. http://dx.doi.org/10.1007/s10853-005-0657-0.

[6] Haanappel VAC, Shemet V, Gross SM, Koppitz T, Menzler NH, Zahid M, et al. Behaviour of various glass–ceramic sealants with ferritic steels under simulated SOFC stack conditions. J Power Sources 2005;150:86–100. http://dx.doi.org/10.1016/j.jpowsour.2005.02.015.

[7] Menzler NH, Sebold D, Zahid M, Gross SM, Koppitz T. Interaction of metallic SOFC interconnect materials with glass–ceramic sealant in various atmospheres. J Power Sources 2005;152:156–67. http://dx.doi.org/10.1016/j.jpowsour.2005.02.072.

[8] Batfalsky P, Haanappel V a C, Malzbender J, Menzler NH, Shemet V, Vinke IC, et al. Chemical interaction between glass–ceramic sealants and interconnect steels in SOFC stacks. J Power Sources 2006;155:128–37. http://dx.doi.org/10.1016/j.jpowsour.2005.05.046.

[9] Menzler NH, Batfalsky P, Blum L, Bram M, Groß SM, Haanappel VAC, et al. Studies of material interaction after long-term stack operation. Fuel Cells 2007;7:356–63. http://dx.doi.org/10.1002/fuce.200700001.

[10] Peng L, Zhu Q. Thermal cycle stability of $BaO–B_2O_3–SiO_2$ sealing glass. J Power Sources 2009;194:880–5. http://dx.doi.org/10.1016/j.jpowsour.2009.06.018.

[11] Chou Y-S, Stevenson JW, Meinhardt KD. Electrical stability of a novel refractory sealing glass in a dual environment for solid oxide fuel cell applications. J Am Ceram Soc 2010;93:618–23. http://dx.doi.org/10.1111/j.1551-2916.2009.03466.x.

[12] Chou Y-S, Stevenson JW, Xia G-G, Yang Z-G. Electrical stability of a novel sealing glass with (Mn,Co)-spinel coated Crofer22APU in a simulated SOFC dual environment. J Power Sources 2010;195:5666–73. http://dx.doi.org/10.1016/j.jpowsour.2010.03.052.

[13] Nielsen KA, Solvang M, Nielsen SBL, Dinesen AR, Beeaff D, Larsen PH. Glass composite seals for SOFC application. J Eur Ceram Soc 2007;27:1817–22. http://dx.doi.org/10.1016/j.jeurceramsoc.2006.05.046.

[14] Wiener F, Bram M, Buchkremer H-P, Sebold D. Chemical interaction between Crofer 22 APU and mica-based gaskets under simulated SOFC conditions. J Mater Sci 2007;42:2643–51. http://dx.doi.org/10.1007/s10853-006-1355-2.

[15] Ogasawara K, Kameda H, Matsuzaki Y, Sakurai T, Uehara T, Toji A, et al. Chemical stability of ferritic alloy interconnect for SOFCs. J Electrochem Soc 2007;154:B657. http://dx.doi.org/10.1149/1.2735919.

[16] Bram M, Niewolak L, Shah N, Sebold D, Buchkremer HP. Interaction of sealing material mica with interconnect steel for solid oxide fuel cells application at 600°C. J Power Sources 2011;196:5889–96. http://dx.doi.org/10.1016/j.jpowsour.2011.02.086.

[17] Thomann O, Rautanen M, Himanen O, Tallgren J, Kiviaho J. Post-experimental analysis of a solid oxide fuel cell stack using hybrid seals. J Power Sources 2015;274:1009–15. http://dx.doi.org/10.1016/j.jpowsour.2014.10.100.

[18] Smeacetto F, Salvo M, Ferraris M, Casalegno V, Asinari P, Chrysanthou A. Characterization and performance of

glass–ceramic sealant to join metallic interconnects to YSZ and anode-supported-electrolyte in planar SOFCs. J Eur Ceram Soc 2008;28:2521–7. http://dx.doi.org/10.1016/j.jeurceramsoc.2008.03.035.
[19] Smeacetto F, Salvo M, Ferraris M, Casalegno V, Asinari P. Glass and composite seals for the joining of YSZ to metallic interconnect in solid oxide fuel cells. J Eur Ceram Soc 2008;28:611–6. http://dx.doi.org/10.1016/j.jeurceramsoc.2007.07.008.
[20] Smeacetto F, Chrysanthou A, Salvo M, Zhang Z, Ferraris M. Performance and testing of glass-ceramic sealant used to join anode-supported-electrolyte to Crofer22APU in planar solid oxide fuel cells. J Power Sources 2009;190:402–7. http://dx.doi.org/10.1016/j.jpowsour.2009.01.042.
[21] Kaur B, Singh K, Pandey OP. Microstructural study of Crofer 22 APU-glass interface for SOFC application. Int J Hydrogen Energy 2012;37:3839–47. http://dx.doi.org/10.1016/j.ijhydene.2011.04.160.
[22] Coillot D, Méar FO, Nonnet H, Montagne L. New viscous sealing glasses for electrochemical cells. Int J Hydrogen Energy 2012;37:9351–8. http://dx.doi.org/10.1016/j.ijhydene.2012.02.194.
[23] Mantel M. Effect of double oxide layer on metal–glass sealing. J Non-Cryst Solids 2000;273:294–301. http://dx.doi.org/10.1016/S0022-3093(00)00137-X.
[24] Chou Y-S, Stevenson JW, Singh P. Effect of pre-oxidation and environmental aging on the seal strength of a novel high-temperature solid oxide fuel cell (SOFC) sealing glass with metallic interconnect. J Power Sources 2008;184:238–44. http://dx.doi.org/10.1016/j.jpowsour.2008.06.020.
[25] Naylor MO, Jin T, Shelby JE, Misture ST. Galliosilicate glasses for viscous sealants in solid oxide fuel cell stacks: Part I: compositional design. Int J Hydrogen Energy 2013;38:16300–7. http://dx.doi.org/10.1016/j.ijhydene.2013.09.121.
[26] Choi JP, Scott Weil K, Matt Chou Y, Stevenson JW, Gary Yang Z. Development of MnCoO coating with new aluminizing process for planar SOFC stacks. Int J Hydrogen Energy 2011;36:4549–56. http://dx.doi.org/10.1016/j.ijhydene.2010.04.110.
[27] Mahapatra MK, Lu K. Seal glass compatibility with bare and (Mn,Co)3O_4 coated AISI 441 alloy in solid oxide fuel/electrolyzer cell atmospheres. Int J Hydrogen Energy 2010;35:11908–17. http://dx.doi.org/10.1016/j.ijhydene.2010.08.066.
[28] Nielsen KA, Dinesen AR, Korcakova L, Mikkelsen L, Hendriksen PV, Poulsen FW. Testing of Ni-plated ferritic steel interconnect in SOFC stacks. Fuel Cells 2006;6:100–6. http://dx.doi.org/10.1002/fuce.200500114.
[29] Fu C, Sun K, Chen X, Zhang N, Zhou D. Effects of the nickel-coated ferritic stainless steel for solid oxide fuel cells interconnects. Corros Sci 2008;50:1926–31. http://dx.doi.org/10.1016/j.corsci.2008.05.001.
[30] Shaigan N, Ivey DG, Chen W. Electrodeposition of Ni/LaCrO [sub 3] composite coatings for solid oxide fuel cell stainless steel interconnect applications. J Electrochem Soc 2008;155:D278. http://dx.doi.org/10.1149/1.2835204.
[31] Shaigan N, Ivey DG, Chen W. Oxidation and electrical behavior of nickel/lanthanum chromite-coated stainless steel interconnects. J Power Sources 2008;183:651–9. http://dx.doi.org/10.1016/j.jpowsour.2008.05.024.
[32] Shong W-J, Liu C-K, Yang P. Effects of electroless nickel plating on 441 stainless steel as SOFC interconnect. Mater Chem Phys 2012;134:670–6. http://dx.doi.org/10.1016/j.matchemphys.2012.03.049.
[33] Shong W-J, Liu C-K, Wu S-H, Liu H-C, Yang P. Oxidation behavior of nickel coating on ferritic stainless steel interconnect for SOFC application. Int J Hydrogen Energy 2014;39:19737–46. http://dx.doi.org/10.1016/j.ijhydene.2014.09.138.
[34] Leonard ME, Amendola R, Gannon PE, Shong W-J, Liu C-K. High-temperature (800 °C) dual atmosphere corrosion of electroless nickel-plated ferritic stainless steel. Int J Hydrogen Energy 2014;39:15746–53. http://dx.doi.org/10.1016/j.ijhydene.2014.07.144.
[35] Garcia-Fresnillo L, Patel R, Niewolak L, Quadakkers WJ, Hua M, Wang Q, et al. Oxidation behaviour and phase transformations of an interconnect material in simulated anode environment of intermediate temperature solid oxide fuel cells. Mater High Temp 2016;3409:1–17. http://dx.doi.org/10.1080/09603409.2016.1244373.
[36] Fakouri Hasanabadi M, Nemati A, Kokabi AH. Effect of intermediate nickel layer on seal strength and chemical compatibility of glass and ferritic stainless steel in oxidizing environment for solid oxide fuel cells. Int J Hydrogen Energy 2015;40:16434–42. http://dx.doi.org/10.1016/j.ijhydene.2015.10.023.
[37] Chou Y-S, Thomsen EC, Williams RT, Choi J-P, Canfield NL, Bonnett JF, et al. Compliant alkali silicate sealing glass for solid oxide fuel cell applications: thermal cycle stability and chemical compatibility. J Power Sources 2011;196:2709–16. http://dx.doi.org/10.1016/j.jpowsour.2010.11.020.
[38] Chou Y-S, Thomsen EC, Choi J-P, Stevenson JW. Compliant alkali silicate sealing glass for solid oxide fuel cell applications: combined stability in isothermal ageing and thermal cycling with YSZ coated ferritic stainless steels. J Power Sources 2012;197:154–60. http://dx.doi.org/10.1016/j.jpowsour.2011.09.027.
[39] Chou Y-S, Choi J-P, Stevenson JW. Compliant alkali silicate sealing glass for solid oxide fuel cell applications: the effect of protective alumina coating on electrical stability in dual environment. Int J Hydrogen Energy 2012;37:18372–80. http://dx.doi.org/10.1016/j.ijhydene.2012.08.084.
[40] Chou Y-S, Thomsen EC, Choi J-P, Stevenson JW. Compliant alkali silicate sealing glass for solid oxide fuel cell applications: the effect of protective YSZ coating on electrical stability in dual environment. J Power Sources 2012;202:149–56. http://dx.doi.org/10.1016/j.jpowsour.2011.11.017.
[41] Singer F, Singer SS. Industrial ceramics. Dordrecht, Netherlands: Springer; 1963. http://dx.doi.org/10.1007/978-94-017-5257-2.
[42] Trejo R, Lara-Curzio E, Shyam A, Kirkham MJ, Garcia-Negron V, Wang Y. Physical and mechanical properties of barium alkali silicate glasses for SOFC sealing applications. Int J Appl Glas Sci 2012;3:369–79. http://dx.doi.org/10.1111/ijag.12004.
[43] Barsoum MW. Fundamentals of ceramics. Bristol: IOP Publishing Ltd; 2003.
[44] Malzbender J, Steinbrech RW. Threshold fracture stress of thin ceramic components. J Eur Ceram Soc 2008;28:247–52. http://dx.doi.org/10.1016/j.jeurceramsoc.2007.05.017.
[45] Persson ÅH Mikkelsen L, Hendriksen PV, Somers MAJ. Interaction mechanisms between slurry coatings and solid oxide fuel cell interconnect alloys during high temperature oxidation. J Alloys Compd 2012;521:16–29. http://dx.doi.org/10.1016/j.jallcom.2011.12.095.
[46] Ling G, He J. The influence of nano-Al_2O_3 additive on the adhesion between enamel and steel substrate. Mater Sci Eng A 2004;379:432–6. http://dx.doi.org/10.1016/j.msea.2004.03.019.
[47] Bodaghi M, Davarpanah A. The influence of cobalt on the microstructure and adherence characteristics of enamel on steel sheet. Process Appl Ceram 2011;5:215–22. http://dx.doi.org/10.2298/PAC1104215B.
[48] Abdullah TK, Petitjean C, Panteix P-J, Rapin C, Vilasi M, Hussain Z, et al. Dissolution equilibrium of chromium oxide

in a soda lime silicate melt exposed to oxidizing and reducing atmospheres. Mater Chem Phys 2013;142:572–9. http://dx.doi.org/10.1016/j.matchemphys.2013.07.055.

[49] Kumar V, Kaur G, Pandey OP, Singh K, Lu K. Effect of thermal treatment on chemical interaction between yttrium borosilicate glass sealants and YSZ for planar solid oxide fuel cells. Int J Appl Glas Sci 2014;5:1–11. http://dx.doi.org/10.1111/ijag.12078.

[50] Paknahad P, Askari M, Ghorbanzadeh M. Application of sol-gel technique to synthesis of copper-cobalt spinel on the ferritic stainless steel used for solid oxide fuel cell interconnects. J Power Sources 2014;266:79–87. http://dx.doi.org/10.1016/j.jpowsour.2014.04.122.

[51] Di Martino J, Rapin C, Berthod P, Podor R, Steinmetz P. Corrosion of metals and alloys in molten glasses. Part 1: glass electrochemical properties and pure metal (Fe, Co, Ni, Cr) behaviours. Corros Sci 2004;46:1849–64. http://dx.doi.org/10.1016/j.corsci.2003.10.024.

[52] Khanna AS. Introduction to high temperature oxidation and corrosion. Materials Park, OH: ASM International; 2002.

[53] Manahan MP. Thermal expansion and conductivity of magnetite flakes taken from the Oconee-2 steam generator. J Mater Sci 1990;25:3424–8. http://dx.doi.org/10.1007/BF00575366.

[54] Tobergte DR, Curtis S. Fe_3O_4: lattice parameters, thermal expansion, density, high temperature phase. Non-tetrahedrally bond. Bin. Compd. II, vol. 53. Berlin/Heidelberg: Springer-Verlag; 2013. p. 1–4. http://dx.doi.org/10.1007/10681735_527.

[55] GILLAM E, HOLDEN JP. Structure of nickel oxide containing alumina. J Am Ceram Soc 1963;46:601–4. http://dx.doi.org/10.1111/j.1151-2916.1963.tb14625.x.

[56] Liu C, Huntz A-M, Lebrun J-L. Investigation on origins of residual stresses in Ni-NiO system by X-ray diffraction at high temperature. Le J Phys IV 1993;3. http://dx.doi.org/10.1051/jp4:19939102. C9-C987–C9-997.

[57] Mougin J, Galerie A, Dupeux M, Rosman N, Lucazeau G, Huntz A-M, et al. In-situ determination of growth and thermal stresses in chromia scales formed on a ferritic stainless steel. Mater Corros 2002;53:486–90. http://dx.doi.org/10.1002/1521-4176(200207)53:7<486::AID-MACO486>3.0.CO;2-P.

[58] Chou Y, Stevenson JW, Hardy J, Singh P. Material degradation during isothermal ageing and thermal cycling of hybrid mica seals under solid oxide fuel cell exposure conditions. J Power Sources 2006;157:260–70. http://dx.doi.org/10.1016/j.jpowsour.2005.07.027.

[59] Eppler RA, Eppler DR. Glazes and glazes coating. Hong Kong: The American Ceramic Society; 2000.

[60] Pampuch R. An introduction to ceramics. London: Springer; 2014.